A Simple Stochastic Model for Generating Broken Cloud Optical Depth and Cloud Top Height Fields

Sergei M. Prigarin[1] and Alexander Marshak[2]

[1] Novosibirsk State University and Institute of Computational Mathematics and Mathematical Geophysics, Russian Academy of Sciences (Siberian Branch), Novosibirsk, Russia

[2] NASA – Goddard Space Flight Center, Climate and Radiation Branch, Maryland, USA

Correspondence

Alexander Marshak

tel. 301-614-6122

email: Alexander.Marshak@nasa.gov

Prepared for publication in

JOURNAL OF THE ATMOSPHERIC SCIENCES

Submitted: December 1, 2007

Revised: May 19, 2008

A Simple Stochastic Model for Generating Broken Cloud Optical Depth and Top Height Fields

Abstract

A simple and fast algorithm for generating two correlated stochastic two-dimensional (2D) cloud fields is described. The algorithm is illustrated with two broken cumulus cloud fields: cloud optical depth and cloud top height retrieved from Moderate Resolution Imaging Spectrometer (MODIS). Only two 2D fields are required as an input. The algorithm output is statistical realizations of these two fields with approximately the same correlation and joint distribution functions as the original ones. The major assumption of the algorithm is statistical isotropy of the fields. In contrast to fractals and the Fourier filtering methods frequently used for stochastic cloud modeling, the proposed method is based on spectral models of homogeneous random fields. For keeping the same probability density function as the (first) original field, the method of inverse distribution function is used. When the spatial distribution of the first field has been generated, a realization of the correlated second field is simulated using a conditional distribution matrix. This paper is served as a theoretical justification to the publicly available software "Simulation of a two-component cloud field" that has been recently released. Though 2D rather than full 3D, stochastic realizations of two correlated cloud fields that mimic statistics of given fields have proved to be very useful to study 3D radiative transfer features of broken cumulus clouds for a better understanding of shortwave radiation and the interpretation of remote sensing retrievals.

1. Introduction

In order to better understand and predict shortwave radiation in realistic cloudy atmospheres, we need to specify the 3D distribution of cloud liquid water. Also, statistical cloud retrievals that include 3D radiative transfer need to be trained on a large number of 3D cloud fields (Evans et al., 2008). Realistic cloud fields and spatial distributions of cloud liquid water can be obtained from either dynamical or stochastic cloud models. Based on cloud dynamics, physical (or dynamical) cloud models such as a large eddy simulation (LES) or a cloud resolving model (e.g., Ackerman et al., 1995) are physically consistent but require specification of a lot of atmospheric parameters and often are computationally expensive. On the other hand, stochastic cloud models based on aircraft, satellite or ground measurements of cloud structure are computationally inexpensive and can output a much larger range of scales than dynamical models. Stochastic cloud models are mostly 2D since currently there are no techniques to measure a full 3D cloud structure. (To get a 3D stochastic model one can assume the same statistics for both horizontal directions (see, Evans and Wiscombe, 2004 and Hogan and Kew, 2005).)

For the last two decades many different cloud stochastic models have been developed. We break them into two classes. The first class of cloud models uses only a few parameters to simulate the main aspects of the realistic cloud fields like mean, standard deviation and correlation often assumed to be a power-law. These models are very simple and are generally used to test hypothesis and better understand cloud-radiation interaction. These are the fractionally-integrated cascade model (Scherzer and Lovejoy, 1987), the bounded cascades (Cahalan, 1994; Marshak et al., 1994), the

fractional Brownian motion (Voss, 1995), the Fourier filtering of Gaussian noise (Barker and Davies, 1992; Evans, 1993; Varnai 2000), the Poisson distribution of cloud elements (Zuev and Titov, 1995) to name a few. These models generally produce an unbroken (overcast) 2D *x-y* field of cloud optical depth or cloud liquid water path. To obtain the desired cloud fraction, a simple threshold can be used (e.g., Barker and Davies, 1992; Marshak et al., 1998).

The second class of cloud stochastic models provides a statistical reconstruction of an observed field and generates the detailed cloud structure. They are also called statistical cloud generators (Venema et al., 2006a, Schmidt et al., 2007). These cloud models are usually 3D rather than 2D. For cumulus clouds, Evans and Wiscombe (2004) used time-height radar data to generate 2D realizations of cloud liquid water that are generalized to 3D fields assuming statistical homogeneity and horizontal isotropy. For stratocumulus clouds, Di Giuseppe and Tompkins (2003) generated 3D cloud liquid water fields combining stochastic horizontal models based on power spectrum and Fourier filtering (at each height) with realistic vertical profiles of total water and temperature. From radar time-height series using Fourier transform technique, Hogan and Kew (2005) generated realistic 3D cirrus clouds with fallstreak structure changing vertically the slope of the power spectrum. Venema et al. (2006a,b) generated a surrogate cloud field with liquid water distribution and spatial correlation (through power spectrum) statistically similar to the observed one. Venema et al., (2006b) also compared radiative properties of LES clouds with its surrogate fields and Venema et al., (2006a) provided an excellent review of different cloud generators. Finally, we mention the Scheirer and Schmidt (2005) generator that reproduced cloud fields of liquid water and

effective radius using aircraft data. Schmidt et al. (2007) used cloud fields simulated by the last three generators as input to a 3D radiative transfer model to compare its output with the radiative flux measurements.

The current paper describes a simple stochastic model that belongs to the second class of cloud stochastic models. For given 2D fields of cloud optical depth and cloud top height, the model generates realizations of these two fields with the same covariance of the cloud mask and the joint distribution as the original fields. In contrast to Evans and Wiscombe (2004), it does not generate 3D cloud liquid water fields but rather provides the *x*-*y* fields of cloud optical and geometrical thicknesses (assuming a constant cloud base). To simulate the required autocorrelation function, it uses spectral models of homogeneous random fields (Prigarin, 1995, 2001) rather than commonly used Fourier filtering (e.g., Evans, 1993; Di Giuseppe and Tompkins, 2003; Evans and Wiscombe, 2004; Hogan and Kew, 2005; Venema et al., 2006b). Another distinguishable feature of this paper is that it provides a theoretical background to the publicly available software that has been recently developed and released by the authors.

The plan of the paper is as follows. The next section briefly discusses two stochastic models of broken cloudiness that are based on a truncated Gaussian homogeneous field. The (auto)correlation function of a 2D field defines its structure. Section 3 describes how to generate a quasi-Gaussian field with a given correlation function that is retrieved from the covariance of the indicator function of the original field. Section 4 then explains how to modify the field to reproduce the observed distribution. Finally in Section 5 we generate the second field using the joint distribution of the given fields of cloud optical depth and cloud top height. Section 6 illustrates the

theory with MODIS data while Section 7 summarizes the main steps of the proposed algorithm and discusses its applications. Section 8 gives a brief summary of the results. At the end, Appendix A demonstrates the relations between the covariance functions of a Gaussian random filed and its indicators, and Appendix B illustrates spectral models of Gaussian isotropic homogeneous random fields on the *x*-*y* plane.

2. Quasi-Gaussian model of broken cloudiness

Let us assume that our cloud field has a constant cloud base at height H_0 and a variable cloud top described by

$$w(x,y) = H_0 + \max\{a[v(x,y) - d], 0\}, \quad -\infty < d < \infty. \tag{1a}$$

Here $v(x,y)$ is a homogeneous Gaussian field with zero mean, unit variance, and a correlation function $K(x,y)$ (with $K(0,0)=1$). The point (x,y,z) belongs to a cloud if $H_0 \le z \le w(x,y)$. A value $w(x,y) = H_0$ simply means that there is a cloud gap in the horizontal point (x,y). The cloud top field w has two parameters: a and d. Parameter $a > 0$ stretches the cloud top field vertically and parameter d defines the truncation level (compare with Marshak et al., 1998).

Simultaneously with Eq. (1a) we consider another model (Kargin and Prigarin, 1988) of cloud top,

$$w(x,y) = H_0 + \max\{a[|v(x,y)| - d], 0\}, \quad 0 \le d < \infty. \tag{1b}$$

We will call Eqs. (1a) and (1b) by model A and B, respectively. Figure 1 illustrates the difference between the two models. We can see that for model A, positive d corresponds to a broken cloud field while negative d rather corresponds to a more "overcast" cloud

with a few gaps. Based on Fig. 1, one can say that model B better represents the cellular structure of stratocumulus while model A is for more broken cumulus clouds.

It can be shown that cloud fraction A_c has a different value for both models, namely:

$$A_c = \mathrm{P}\{v(x,y)>d\} = 1 - \Phi(d),\ -\infty < d < \infty \tag{2a}$$

for model A,

$$A_c = \mathrm{P}\{v(x,y)>d\} = 2[1 - \Phi(d)],\ 0 \le d < \infty \tag{2b}$$

for model B, where

$$\Phi(d) = \frac{1}{\sqrt{2\pi}} \int_{-\infty}^{d} \exp(-\frac{x^2}{2}) dx$$

is the standard normal cumulative distribution function which ranges between 0 and 0.5 for negative d and between 0.5 to 1 for the positive ones.

For both models we can determine the average number of clouds m_c per unit area as a limit of number of clouds in a convex domain of area S divided by S when S tends to infinity. Note that m_c is dimensionless. Obviously m_c will depend on d and autocorrelation function K. For isotropic fields, one obtains (e.g., Sveshnikov, 1968, Eq. (45.51), pg. 441)

$$m_c = i \frac{d}{\sqrt{(2\pi)^3}} k \exp(-\frac{d^2}{2}),\quad d > 0 \tag{3}$$

where i=1 for model A and i=2 for model B. Here $k > 0$ is the second derivative of $-K(x,y)$ with respect to x or y taken at x=y=0 (with sign '-'). Note that for isotropic fields, the derivatives are equal (see Eq. (5) below).

Figure 2 shows the dependence of m_c on cloud fraction A_c for both models and isotropic fields. We see that the number of clouds first increases with cloud fraction and then decreases. This is because cloud fraction A_c itself monotonically decreases with the truncation level d while number of clouds m_c first increases with d then decreases (see Fig. 1). Note that for model A, number of clouds m_c for $A_c > 0.5$ ($d<0$) is not defined. Generalization of Eq. (3) to anisotropic fields is straightforward (Prigarin and Marshak, 2005).

To summarize, both cloud models A and B are uniquely determined by parameters a and d and a correlation function K. To simulate a cloud field with a given cloud fraction A_c, we first solve Eq. (2) for the truncation level d. Then one needs to generate the correlation function $K(x,y)$ based on some additional information on correlation in a real cloud field. Parameter a is determined from a simple one-point statistics of the cloud top field. The most difficult part of such an approach is the choice (or generation) of the correlation function K; it will be discussed in the next section.

Finally, we emphasize that the cloud top height field $w(x,y)$ is simulated in two steps: (*i*) simulation of the Gaussian field $v(x,y)$ with mean zero and correlation function $K(x,y)$, and (*ii*) calculation of $w(x,y)$ with parameters a and d using (1a) or (1b). The problem of numerical simulation of Gaussian random fields has been well studied (e.g., Chapters 1, 2, 4 in Ogorodnikov and Prigarin (1996) and Prigarin (2001) and references therein) and will not be discussed here. Appendix B illustrates the approximation of a Gaussian homogeneous random field used in the numerical examples in Section 6.

3. Correlation function

The correlation function defines the geometrical structure of a cloud field, the size and distribution of individual clouds and space between them. Perhaps the simplest and/or the most deterministic isotropic cloud field used in the first stochastic models can be defined by a Bessel function of the first kind, J_0 (see, Gikhman and Skorokhod, 1977, pg. 87). In this case, the correlation function

$$K(x,y) = J_0(\rho\sqrt{x^2+y^2}) \tag{4}$$

where parameter ρ is responsible for cloud sizes (the larger ρ the smaller an average cloud is.) It is easy to see that

$$k = -\frac{\partial^2 K(x,y)}{\partial x^2}\bigg|_{x=y=0} = -\frac{\partial^2 K(x,y)}{\partial y^2}\bigg|_{x=y=0} = \frac{\rho^2}{2}. \tag{5}$$

Thus to define ρ, one uses Eq. (3) that relates the average number of clouds per unit area, m_c, and second derivative k. Because ρ is fixed, the use of correlation function (4) is very limited and cloud fields based on it are unrealistic (see Fig. 3 as an example).

To generalize (4), Prigarin et al. (1998) used the radial spectral density of a Gaussian field, $z(\rho)$, and a representation of the normalized correlation function as an integral over all cloud sizes ρ of a product between $z(\rho)$ and J_0,

$$K(x,y) = \int_0^\infty J_0(\rho\sqrt{x^2+y^2})z(\rho)d\rho. \tag{6}$$

Here, $z(\rho) \geq 0$ and $\int_0^\infty z(\rho)d\rho = 1$. Varying $z(\rho)$, in general, one can get "any" correlation function of a random isotropic field on the plane.

Below we briefly describe a general procedure of generating correlation function $K(x,y)$ based on observations leaving the details for Appendix A. As an illustration, in Section 6 we apply our algorithm to a broken cloud scene retrieved from Moderate Resolution Imaging Spectrometer (MODIS).

Let $I(x,y)$ be an indicator function (a binary cloud mask) that takes value 1, if there is a cloud above point (x,y), and 0 otherwise. Based on observations, we can estimate the mathematical expectation of I, which is a cloud fraction A_c, i.e.,

$$A_c = \mathrm{E}[I(x,y)] \tag{7}$$

and its covariance function,

$$\mathrm{K_I}(x,y) = \mathrm{E}[I(x,y)\, I(0,0)] \,. \tag{8}$$

It is known (Ogorodnikov and Prigarin, 1996, pg. 65) that the covariance function $\mathrm{K_I}(x,y)$ of the indicator field $I(x,y)$ and correlation function $K(x,y)$ of a Gaussian field $v(x,y)$ are nontrivially related. This relationship allows us to retrieve correlation function $K(x,y)$ from the measured covariance function $\mathrm{K_I}(x,y)$. The main steps of the retrieval are described in Appendix A. Note that the truncation level d is uniquely defined from Eqs. (2) and (7).

4. Geometrical thickness with a given density

Equations (1a) and (1b) alone do not allow us to control the distribution of cloud geometrical thickness, $w(x,y)$-H_0. Determined by Eqs. (1a) and (1b), this distribution is a scaled up ($a > 1$) or down ($a < 1$) truncated (by a parameter d) Gaussian distribution; its density is defined by

$$f_a(h) = \frac{1}{aC}\varphi(\frac{h}{a} + d), \quad h > 0, \quad C = \int_d^\infty \varphi(x)dx \tag{9}$$

where $\varphi(x) = \frac{1}{2\pi}\exp(-x^2/2)$ is a standard Gaussian density. However, the observed distribution of cloud thickness does not necessarily satisfy Eq. (9). In general, one has to modify Eqs. (1a) and (1b) in order to reproduce the observed distribution. We describe below a modification of a Gaussian model that allows reproduction of any given distribution. This modification is based on the method of inverse distribution function widely used in statistical modeling (e.g., Ogorodnikov and Prigarin, 1996, pg. 65-71).

Let $g(h)$ ($h > 0$) be a density of the observed distribution of cloud thickness. We denote its distribution function by

$$G(h) = \int_0^h g(x)dx, h > 0\,. \tag{10}$$

It is easy to see that if

$$F(h) = \int_0^h f_1(x)dx, h > 0 \tag{11}$$

is the distribution function with density $f_1(h)$ defined in Eq. (9) with a = 1 and ξ is a random variable distributed with the density f_1 then $G^{-1}F(\xi)$ will have a density of the observed distribution of cloud geometrical thickness. Indeed, there is a general statement (e.g., Gentle, 2003, p. 42): if F is a distribution function of a random variable ξ then $F(\xi)$ is uniformly distributed on the interval (0,1). Therefore, the random variable $G^{-1}F(\xi)$ has the probability density g. (Note that the method of inverse distribution function similar to

the above has been also used by Evans and Wiscombe (2004) to generate lookup tables for cloud liquid water content and droplet effective radius (see their Eq. (A.3).)

This leads us to the following modification of Eqs. (1a) and (1b):

$$w(x,y) = H_0 + G^{-1}F\left[\max\{v(x,y) - d, 0\}\right], \quad -\infty < d < \infty \tag{12a}$$

for model A, and

$$w(x,y) = H_0 + G^{-1}F\left[\max\{|v(x,y)| - d, 0\}\right], \quad 0 \le d < \infty . \tag{12b}$$

for model B.

In contrast to (1a) and (1b), distributions of cloud thickness $w(x,y)$-H_0 defined by either (12a) or (12b) match the observed probability distribution $G(h)$. In addition, we recall that $v(x,y)$ is a homogeneous Gaussian field with zero mean and unit variance; its correlation function $K(x,y)$ is retrieved from the covariance function $K_I(x,y)$ of the observed cloud mask field $I(x,y)$. For both models, parameter d is uniquely determined from the average value of $I(x,y)$, i.e. cloud fraction A_c (see (7)).

5. Joint distribution of optical and geometrical thicknesses

We assume here that we have two random variables: cloud optical depth $\tau(x,y)$ and cloud geometrical thickness $h(x,y)$. Then a pair (τ,h) will be a two-dimensional variable and $P(\tau_1 < \tau < \tau_2,\ h_1 < h < h_2)$ will be the probability that the values of τ and h fall in the intervals (τ_1,τ_2) and (h_1,h_2), respectively.

Practically (see next section), when two matrixes τ and h are given from observations, we first subdivide all their values into M and N bins, respectively. Then we calculate a conditional distribution matrix,

$$P(m,n) = P(\tau \text{ is in } m\text{'s bin} \mid \text{provided } h \text{ is in } n\text{'s bin}),\ m=1,\ldots,M;\ n=1,\ldots,N. \qquad (13)$$

Now, if we assume that we have a realization of one variable, say h, then using the conditional distribution matrix P we can simulate a distribution of a second variable, τ. This is a straightforward procedure similar to a simulation of random number with a given distribution. As a result for each point (x,y) we will get both $\tau(x,y)$ and $h(x,y)$ preserving conditional distribution (13) as well as the distribution of the random vector $(h(x,y), \tau(x,y))$. The order of simulation (first τ and then h or first h and then τ) is irrelevant for the reproduction of the joint distribution of the components of this two-dimensional vector.

Note that realizations of the second component generated using a conditional distribution matrix (13) are usually more stochastic (or noisy) than the given one. This is especially well pronounced if the original field has a strong spatial heterogeneity, e.g. the highest values are localized in several neighboring pixels. In a simulated field, these high values are not necessarily well localized and sometimes can be distributed through the whole scene making it much noisier. This problem has been discussed in more details in Prigarin and Marshak (2008).

6. Illustration with MODIS data

To illustrate the above theory with observations, we have selected a 1 km spatial resolution MODIS 68 km by 68 km broken cumulus cloud scene (Fig. 4a) from a less polluted region in Brazil, centered at 17° S and 42° W. The data were acquired on August 9, 2001 at 10:15 am local time. The solar zenith angle θ_0=41°. This scene is part of the International Comparison of 3D Radiative Transfer Codes (I3RC) phase 3 (Cahalan et al., 2005) and has been used for the analysis of the retrieved droplet size by Marshak et al. (2006) and for the radiative effects of broken clouds on aerosol retrievals by Wen et al. (2007). Cloud fraction in the scene, A_c=0.4. The MODIS image is collocated with a high spatial resolution (15 m) Advanced Spaceborne Thermal Emission and Reflection Radiometer (ASTER) image (Yamagushi et al., 1998) plotted in Fig. 4b. The solar azimuth angle φ_0=23° (from upper right corner) as can be confirmed from the casting of the shadows.

In panel (c) and (d) we have also added the retrieved cloud optical depth and cloud top height at a 1 by 1 km resolution. While the retrieved 1 by 1 km cloud optical depth is an operational MODIS product, the operational cloud top height retrievals have a 5 by 5 km resolution (Platnick, et al. 2003). To estimate the 1 by 1 km resolution of cloud top height, we used the brightness temperature at 11 μm (MODIS band 31) (see Wen et al., 2007 for details). As a result, panels (c) and (d) will be served as the basic scenes for our illustration.

First, Fig. 5a shows the indicator function $I(x,y)$ of the cloud optical depth field from panel 4c. Cloud fraction, as a mathematical expectation of I defined in (7), will be 0.4. The right panel, Fig. 5b, is the indicator function of a realization of a simulated field

that has the same covariance function $K_I(x,y)$ as the measured one. As shown in Appendix A, to get $K(x,y)$ we first estimated the covariance function K_I defined in (8) and then retrieved $K(x,y)$ with the help of the Owen function (Prigarin et al., 2004).

Next we illustrate how the distribution of cloud optical depth can be reproduced using Eq. (12a). This is done for Model A which is, perhaps, better agrees with the results of observations than model B (Prigarin and Marshak, 2005). Four realizations of cloud optical depth distribution are plotted in Fig. 6. All of them have approximately the same covariance function $K_I(x,y)$ of the indicator field (see Fig. 7) and probability density function $g(\tau)$ as the original cloud optical depth field shown in Fig. 5c. Figure 8 illustrates these five pdfs: the original one and the four realizations of cloud optical depth from Fig. 6.

Now we illustrate the joint distribution of optical depth and cloud top height. Figure 9 shows a joint distribution function while Fig. 10 shows an example of two conditional distributions $F(h|\tau)$ for $\tau=3.5\pm0.5$ and $\tau=10\pm1$. The conditional distributions of cloud top height h are obviously different. Finally, Fig. 11 for the realization of cloud optical depth plotted in Fig. 6b shows three realizations of cloud top height. As we can see from Fig. 12 their pdfs match (approximately) the original pdf of cloud top height from Fig. 4d.

7. Main steps of the model

Based on the above description, the software "Simulation of a two-component cloud field" that generates realizations of cloud optical depth and cloud top height from given observations have been developed and is freely available for download from

http://i3rc.gsfc.nasa.gov/Public_codes_clouds.htm (click on *PDF-based stochastic cloud model*).

Let us summarize here the main steps of the simulation procedure. There are only two input files: cloud optical depth $\tau(x,y)$ and cloud geometrical thickness $h(x,y)$ (as shown in Figs. 4c and 4d). The main 11 steps are the following:

1. Read input file $\tau(x,y)$;
2. Estimate cloud fraction A_c, see (7);
3. Find the truncation level d from (2);
4. Estimate covariance function of the indicator field K_I, see (8);
5. Compute correlation function K, see Appendix A;
6. Generate a Gaussian homogeneous random field $v(x,y)$ with mean zero and correlation function K, see Appendix B;
7. Simulate $\tau^*(x,y)$ modifying the Gaussian field according to (12);
8. Read input file $h(x,y)$;
9. Calculate joint distribution of τ and h fields, see Fig. 9;
10. Calculate a conditional distribution matrix (13);
11. Using the conditional distribution matrix, simulate realization $h^*(x,y)$ that corresponds to realization $\tau^*(x,y)$ generated at step 7, see Fig. 11.

In the software, the first 7 steps are accomplished by the executable file **0x-sp-a-s.exe**. The input file is matrix $\tau(x,y)$. The output files are: a realization $\tau^*(x,y)$ of cloud optical depth field, the estimated covariance function of the indicator field, the computed autocorrelation function of the Gaussian field and histograms of the input and output

optical depth fields. The executable file **DISTR-M2.exe** estimates a joint distribution function of two random fields $\tau(x,y)$ and $h(x,y)$. The output files of this program are the joint and conditional distributions (steps 8-10). For the last step, the executable file **X_Ysim.exe** is used. It provides a realization $h^*(x,y)$ of cloud top height field. In that way, the realizations $\tau^*(x,y)$ and $h^*(x,y)$ imitate the input fields $\tau(x,y)$ and $h(x,y)$ reproducing the covariance function of the indicator field and joint distribution of τ and h components for two-dimensional vectors $(\tau(x,y), h(x,y))$. Note, that here the random fields are assumed to be statistically homogeneous and isotropic.

8. Summary

Cloud stochastic models proved to be an important tool to study 3D radiative effects in clouds, especially in broken cumulus clouds (e.g., Barker and Davies, 1992, Evans, 1993, Marshak et al., 1998, Varnai, 2000, Evans and Wiscombe, 2004, Schmidt et al. 2007). Here we have provided a theoretical description of a simple algorithm that generates realizations of the two correlated stochastic two-dimensional (2D) cloud fields that have similar statistical characteristics as given cloud fields. Each step of the algorithm has been illustrated with two broken cumulus cloud fields: cloud optical depth and cloud top height retrieved from MODIS. While most stochastic cloud models use Fourier filtering of Gaussian signal to generate the required correlation (e.g., Schertzer and Lovejoy, 1987; Evans, 1993; Di Giuseppe and Tompkins, 2003; Evans and Wiscombe, 2004; Hogan and Kew, 2005; Venema et al., 2006b), our algorithm is based on spectral models of homogeneous random fields (Prigarin, 1995, 2001). A nonlinear transformation of Gaussian functions (the method of inverse distribution function) allows

us to keep distribution function similar to the one of the first original field. Realizations of the correlated second field are generated using a conditional distribution matrix.

This paper is accompanied by the software "Simulation of a two-component cloud field" that has been recently released and can be freely downloaded from http://i3rc.gsfc.nasa.gov/Public_codes_clouds.htm. The software generates a two-component cloud field and provides programs to simulate two-dimensional distributions. The software contents a program (**0x-sp-a-s**) that generates realizations of a broken cloud field (X) with similar statistical characteristics (autocorrelation, density, and indicator functions) as the first given sample, a program (**DISTR-M2**) that estimates joint and conditional distributions for the two given samples and a program (**X_Ysim**) that simulates sample Y while the sample X is given. At present, the software runs only on Windows PCs but will be later extended to other platforms.

Finally we note that this model is a 2D stochastic model rather than 3D. To extend it to a 3D cloud model, we need to assume a vertical profile of cloud liquid water (see, Di Giuseppe and Tompkins, 2003). A simple linear increase of liquid water with height can be easily implemented in the frame of this model on its next stage.

Acknowledgments. Both S. Prigarin and A. Marshak have been supported by the NSF Collaboration in Basic Science and Engineering (COBASE) travel grant. S. Prigarin has been also supported by INTAS (Grant 05-1000008-8024), RFBR (Grant 06-05-64484) and the President's program Leading Scientific Schools (Grant NSh-4774.2006.1). A. Marshak has been supported by the Department of Energy (under grant DE-A105-90ER61069 to NASA's GSFC) as part of the Atmospheric Radiation Measurement

(ARM) program and by NASA's Radiation Program Office (under grants 621-30-86 and 622-42-57). We thank Dr. Tamas Varnai for his help with testing the software and Dr. Warren Wiscombe for stimulating the development of stochastic models of broken cloud fields. We are grateful to 2 anonymous reviewers and Dr. Sebastian Schmidt, for the excellent job they did reviewing the paper.

Appendix A. Relations for covariance functions of a Gaussian random filed and its indicators

Assume that $v(x,y)$ is a homogeneous Gaussian random field on the plane with mean zero and correlation function $K(x,y)=E[v(x,y)\, v(0,0)]$. Let us consider two indicator fields with respect to a fixed level d:

$$I^{(1)}(x,y)=\begin{cases}0 & \text{for } v(x,y)<d\\ 1 & \text{otherwise}\end{cases}, \qquad I^{(2)}(x,y)=\begin{cases}0 & \text{for } |v(x,y)|<d\\ 1 & \text{otherwise}\end{cases}.$$

These indicators correspond to Model A (1a) and Model B (1b) introduced in Section 2. In this Appendix we present the basic relations between covariance functions of the random field $v(x,y)$ and its indicators (for details, see Prigarin et al., 2004). For the covariance functions $K_I^{(n)}(x,y)=E[I^{(n)}(x,y)\, I^{(n)}(0,0)]=P\{I^{(n)}(x,y)=1,\, I^{(n)}(0,0)=1\}$ we have

$$K_I^{(n)}(x,y) = R^{(n)}(K(x,y)), \tag{A1}$$

where

$$R^{(1)}(r) = \int\limits_{\{\xi>d\}}\int\limits_{\{\eta>d\}} \varphi_r(\xi,\eta)\,d\xi d\eta \qquad R^{(2)}(r) = \int\limits_{\{|\xi|>d\}}\int\limits_{\{|\eta|>d\}} \varphi_r(\xi,\eta)\,d\xi d\eta \tag{A2}$$

and

$$\varphi_r(\xi,\eta) = \left[2\pi\sqrt{1-r^2}\,\exp\left(\frac{\xi^2+\eta^2+2r\xi\eta}{2(1-r^2)}\right)\right]^{-1} \tag{A3}$$

is the probability density of a two-dimensional Gaussian random vector with zero mean, unit variance of the components and correlation coefficient r between the components.

To find the correlation function $K(x,y)$ of the Gaussian random field for a quasi-Gaussian model of broken clouds it is necessary to estimate function $K_I^{(n)}(x,y)$ that is the

covariance function of the cloud indicator field and to solve numerically equation (A1) (n=1 for Model A and n=2 for Model B). For computations it is reasonable to use the following representations of (A2) in terms of Owen's function:

$$R^{(1)}(r) = \Phi(-d)-2T(d,a), \qquad R^{(2)}(r) =4\Phi(-d)-4[T(d,a)+T(d,1/a)], \tag{A4}$$

where Φ is the standard normal cumulative distribution function, $a = \sqrt{(1-r)/(1+r)}$ and

$$T(d,a) = \frac{1}{2\pi}\int_0^a \exp\left[-d^2(1+u^2)/2\right]\frac{du}{1+u^2} \tag{A5}$$

is Owen's function.

Appendix B. On simulation of a Gaussian homogeneous isotropic field with a given correlation function

Here we briefly present a numerical method used in the software "Simulation of a two-component cloud field" for modeling Gaussian random fields on a plane (for details see Chapter 2 in Ogorodnikov and Prigarin (1996), Chapter 1, and particularly Section 1.1.4, in Prigarin (2001) and Prigarin and Titov (1996)). To simulate a Gaussian homogeneous isotropic random field *v(x,y)* with mean zero and correlation function $K(x,y)$ we use an approximation of the following type:

$$v^{JM}(x,y) = M^{-1/2} \sum_{j=1}^{J} c_j \sum_{m=1}^{M} \sqrt{-2\ln\alpha_{km}}\ \cos(x\rho_j \cos\omega_{jm} + y\rho_j \sin\omega_{jm} + 2\pi\beta_{jm}),$$

where

$$\rho_j = (j+0.5)B/J, \qquad c_j^2 = \int_{(j-1)B/J}^{jB/J} z(\rho)d\rho,$$

$$\omega_{jm} = \pi(m+\gamma_j)/M, \qquad z(\rho) = \rho\int_0^{\infty} rJ_0(r\rho)K\ (r)dr,$$

$\alpha_{jm}, \beta_{jm}, \gamma_j$ are independent random variables uniformly distributed in (0,1), and the same symbol K is used for the correlation function (of the isotropic field) depending on a point on the plane (x,y) and on the distance $r = \sqrt{x^2+y^2}$: $K(r)=K(x,y)$. Function $z(\rho)$ is the *radial spectral density* (see (6) in section 3). Such numerical models are called *spectral models* because they approximate stochastic integrals in the spectral decomposition of the random field

$$v(x,y) = \int_0^{+\infty}\int_{-\infty}^{+\infty} \cos(\lambda x + \nu y)\xi(d\lambda\, d\nu) + \int_0^{+\infty}\int_{-\infty}^{+\infty} \sin(\lambda x + \nu y)\eta(d\lambda\, d\nu)$$

by finite sums. Here $\xi(d\lambda d\nu)$ and $\eta(d\lambda d\nu)$ are the orthogonal stochastic measures. (For the details on the spectral decompositions see, e.g., Gikhman and Skorokhod (1977, p.

273).) The spectral model is a sum of JxM random harmonics and it depends on three parameters J, M and B where B is an upper boundary of the radial spectrum of the model. (In the accompanied software "Simulation of a two-component cloud field", parameters J and M are chosen manually, while B is specified automatically). Additional information on construction, properties, errors and convergence of spectral models can be found in Prigarin (2001).

References

Ackerman, A. S., O. B. Toon, and P. V. Hobbs, 1995: A model for particle microphysics, turbulent mixing, and radiative transfer in the stratocumulus-topped marine boundary layer and comparisons with measurements. *J. Atmos. Sci.*, **52**, 1204–1236.

Barker, H. and J. A. Davies, 1992: Solar radiative fluxes for stochastic, scale-invariant broken cloud fields. *J. Atmos. Sci.*, **49**, 1115-1126.

Cahalan, R. F., 1994: Bounded cascade clouds: Albedo and effective thickness. *Nonlinear Processes in Geoph.*, **1**, 156–167.

Cahalan R.F, L. Oreopoulos, A. Marshak, K.F. Evans, A.B. Davis, R. Pincus, K. Yetzer, B. Mayer, R. Davies, T.P. Ackerman, H.W. Barker, E.E. Clothiaux, R.G. Ellingson, M.J. Garay, E. Kassianov, S. Kinne, A. Macke, W. O'Hirok, P.T. Partain, S.M. Prigarin, A.N. Rublev, G.L. Stephens, F. Szczap, E.E. Takara, T. Várnai, G. Wen, and T.B. Zhuravleva, 2005. The International Intercomparison of 3D Radiation Codes (I3RC): Bringing together the most advanced radiative transfer tools for cloudy atmospheres. *Bulletin Amer. Meteor. Soc. (BAMS),* **86**, 1275-1293.

Di Giuseppe, F., and A.M. Tompkins, 2003: Effect of spatial organization on solar radiative transfer in 3D idealized stratocumulus cloud fields. *J. Atmos. Sci.*, **60**, 1774-1794.

Evans, K.F., 1993: A general solution for stochastic radiative transfer. *Geoph. Res. Lett.*, **20**, 2075–2078.

Evans, K.F., and W.J. Wiscombe, 2004: An algorithm for generating stochastic cloud fields from radar profile statistics. *Atmos. Res.*, **72**, 263–289.

Evans, K.F., A. Marshak, and T. Varnai, 2008. The potential for improved cloud optical depth retrievals from the multiple directions of MISR. *J. Atmos. Sci.*, (in press).

Gentle J.E., 2003 *Random Number Generation and Monte Carlo Methods*, Springer, 2nd ed., 381 p.

Gikhman I.I. and A.V. Skorokhod, 1977: *An Introduction to the Theory of Random Processes*. Nauka, Moscow [in Russian].

Hogan, R. J. and S. F. Kew, 2005: A 3D stochastic cloud model for investigating the radiative properties of inhomogeneous cirrus clouds. *Q. J. R. Meteorol. Soc.*, **131**, 2585-2608.

Kargin, B.A. and Prigarin, S.M., 1988: Modelling of stochastic fields of heap clouds and study of their radiative properties with Monte Carlo method. Preprint No. 817. Compt. Cent. Sib. Division, USSR Acad. Sci., Novosibirsk, 1988 [in Russian].

Marshak, A., A. Davis, R.F. Cahalan, and W.J. Wiscombe, 1994: Bounded cascade models as non-stationary multifractals. *Phys. Rev. E*, **49**, 55–69.

Marshak, A., A. Davis, W.J. Wiscombe, W. Ridgway, and R.F. Cahalan, 1998: Biases in shortwave column absorption in the presence of fractal clouds. *J. Climate*, **11**, 431–446.

Marshak, A., S. Platnick, T. Várnai, G. Wen, and R. F. Cahalan, 2006. Impact of 3D radiative effects on satellite retrievals of cloud droplet sizes. *J. Geophys. Res.*, **111**, D09207 doi: 10.1029/2005JD006686.

Ogorodnikov, V.A. and S.M. Prigarin, 1996: *Numerical Modelling of Random Processes and Fields: Algorithms and Application*s, VSP, Utrecht, the Netherlands, 240 p.

Platnick, S., M. D. King, S. A. Ackerman, W. P. Menzel, B. A. Baum, J. C. Riedi, and R. A. Frey, 2003: The MODIS cloud products: Algorithms and examples from Terra. *IEEE Trans. Geosci. Remote Sens.*, **41** (2), 459-473.

Prigarin S.M., 1995: Spectral models of random fields and their applications. *Advances in modelling and analysis*, A, **29**, 2, 39-51

Prigarin, S.M., 2001: *Spectral Models of Random Fields in Monte Carlo Methods*, VSP, Utrecht, 198p.

Prigarin, S. M., B.A. Kargin, and U.G. Oppel, 1998: Random fields of broken clouds and their associated direct solar radiation, scattered transmission, and albedo. *Pure and Applied Optics, A*, **7**, 1389-1402.

Prigarin, S.M., A. Martin, G. Winkler, 2004: Numerical models of binary random fields on the basis of thresholds of Gaussian functions, *Siberian J. of Num. Math.*, **7**, 165-175.

Prigarin, S., and A. Marshak, 2005. Numerical model of broken clouds adapted to observations. *Atmos. and Oceanic Optics*, **18**, 256-263.

Prigarin, S. and A. Marshak, 2008. Simulation of vector semi-binary homogeneous random fields and modeling of broken clouds. *Siberian J. Numeric. Anal.*, (in press).

Prigarin, S. M. and G.A. Titov, 1996. Spectral methods of numerical modeling of geophysical fields. *Atmospheric and Oceanic Optics*, **9**, 629-635.

Scheirer R. and S. Schmidt, 2005: CLABAUTAIR: A new algorithm for retrieving three-dimensional cloud structure from airborne microphysical measurements. *Atmos. Chem. Phys.* **5**: 2333–2340.

Schertzer, D., and S. Lovejoy, 1987: Physical modeling and analysis of rain and clouds by anisotropic scaling multiplicative processes. *J. Geophys. Res.*, **92**, 9693-9714.

Schmidt, K.S., V. Venema, F. Di Giuseppe, R. Scheirer, M. Wendisch, and P. Pilewski., 2007: Reproducing cloud microphysics and irradiance measurements using three 3D cloud generators. *Q.J.R. Meteorol. Soc.*, **133**, 765-780.

Sveshnikov, A. A., 1968. *Applied Methods in Random Function Theory*. Nauka, Moscow, 463 pp. (in Russian)

Várnai, T., 2000: Influence of three-dimensional radiative effects on the spatial distribution of shortwave cloud reflection. *J. Atmos. Sci.*, **57**, 216–229.

Venema, V., S. Bachner, H.W. Rust, and C. Simmer, 2006a: Statistical characteristics of surrogate data based on geophysical measurements, *Nonlin. Proc. Geophys.*, **13**, 449–466.

Venema, V., S. Meyer, S.G. Garcia, A. Kniffka, C. Simmer, S. Crewell, U. Löhnert, T. Trautmann and A. Macke, 2006b: Surrogate cloud fields generated with the iterative amplitude adapted Fourier transform algorithm, *Tellus.*, **58A**, 104–120.

Voss, R., 1985. Random fractal forgeries. In R.A. Earnshaw, editor, *Fundamental Algorithms in Computer Graphics*, pages 805-835. Springer-Verlag.

Wen, G., A. Marshak, R.F. Cahalan, L.A. Remer, and R.G. Kleidman, 2007. 3-D aerosol-cloud radiative interaction observed in collocated MODIS and ASTER images of cumulus cloud fields, *J. Geophys. Res.*, **112**, D13204, doi:10.1029/2006JD008267.

Zuev V.E. and G.A. Titov, 1995: Radiative transfer in cloud fields with random geometry. *.J Atmos. Sci.*, **52**, 176-190.

Figure Captions

Figure 1. A schematic illustration of models A and B. H_0 is a constant cloud base, d is a cutting threshold level.

Figure 2. Number of clouds per unit area, m_c (k=1), as a function of cloud fraction A_c for both models A and B.

Figure 3. Configuration of cloud fields (300 km by 300 km) for model A (left) and model B (right) on the basis of a Gaussian random field with correlation function J_0 for the same cloud fraction A_c=0.58 (ρ=0.5; d= -0.20 for model A, and d=0.55 for model B). To simulate a Gaussian random field a spectral model from Prigarin, 2001 (Section 1.1.4) was used (see also Appendix B).

Figure 4. A 68 km by 68 km region in Brazil centered at 17° S and 42° W collected on August 9, 2001 at 1015 local time. The solar zenith angle $\theta_0=41^0$; the solar azimuth angle φ_0=23° (from the top). **(a)** MODIS true color RGB 1 km resolution; **(b)** ASTER RGB 15 m resolution; **(c)** retrieved cloud optical thickness; **(d)** retrieved cloud top height (in km).

Figure 5. Indicator functions $I(x,y)$ of a cloud field: white is cloud (I=1) while black is a cloud-free area (I=0). Cloud fraction A_c=0.4. (**Left**) 68 km by 68 km MODIS image centered at (17.1° S,42.16°W) acquired on August 9, 2001. (**Right**) a realization of a simulated field.

Figure 6. Four realizations of cloud optical depth; all of them have the same covariance function of the cloud mask $K_I(x,y)$ and histogram $g(\tau)$ as the one in Fig. 4c. Color scale is the same as in Fig. 4c. The size of the images is the same as in Fig. 5: 68 km by 68 km.

Figure 7. Estimates of covariance function $K_I(x,y)=K_I(r)$ ($r = \sqrt{x^2 + y^2}$) of the indicator function $I(x,y)$ for the observed (solid line) and simulated (dot line) cloud fields from Fig. 5.

Figure 8. The original histogram $g(\tau)$ and four other histograms that correspond to four realizations of cloud optical depth shown in Fig. 6.

Figure 9. Joint distribution of the given cloud optical depth and cloud top height fields.

Figure 10. The conditional distribution function $F(h|\tau)$ used to simulate cloud top height h. $F(h|\tau)$ is shown for two values of optical depth τ.

Figure 11. (**a**) One realization of cloud optical depth from Fig. 6b. (**b**)-(**d**) Three realizations of cloud top height distribution; they correspond to the cloud optical depth field shown in panel (a). All realizations have the same conditional distribution $F(h|\tau)$.

Figure 12. A probability density function (pdf) of three realizations of cloud top height shown in Fig. 11. The original pdf of cloud top height from Fig. 4d is also shown.

FIGURES

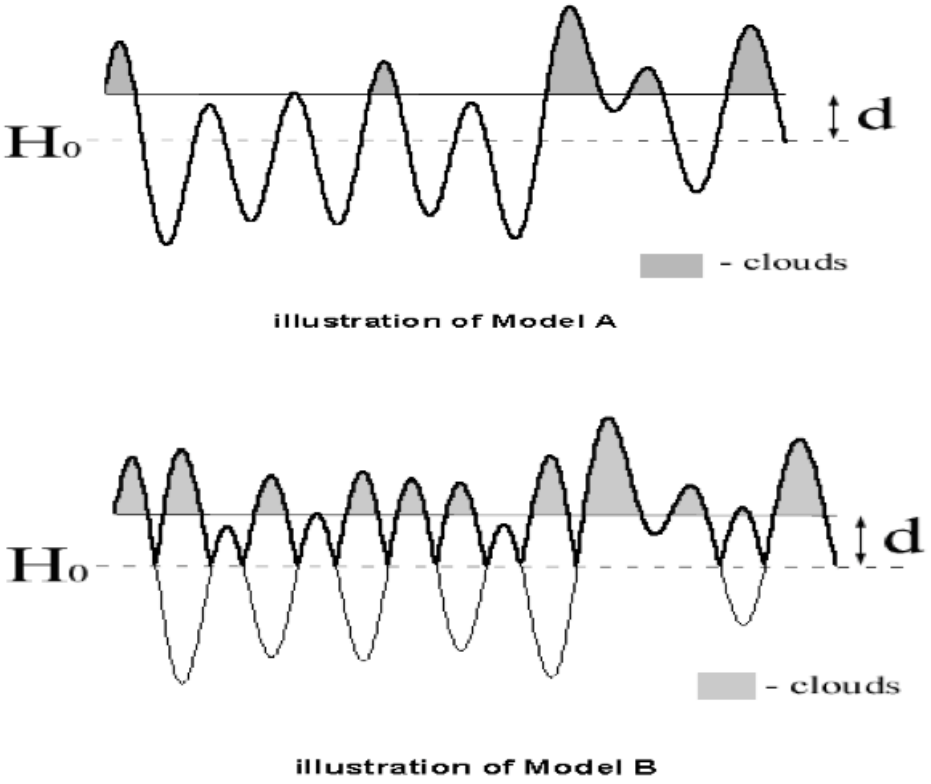

Figure 1. A schematic illustration of models A and B. H_0 is a constant cloud base, d is a cutting threshold level.

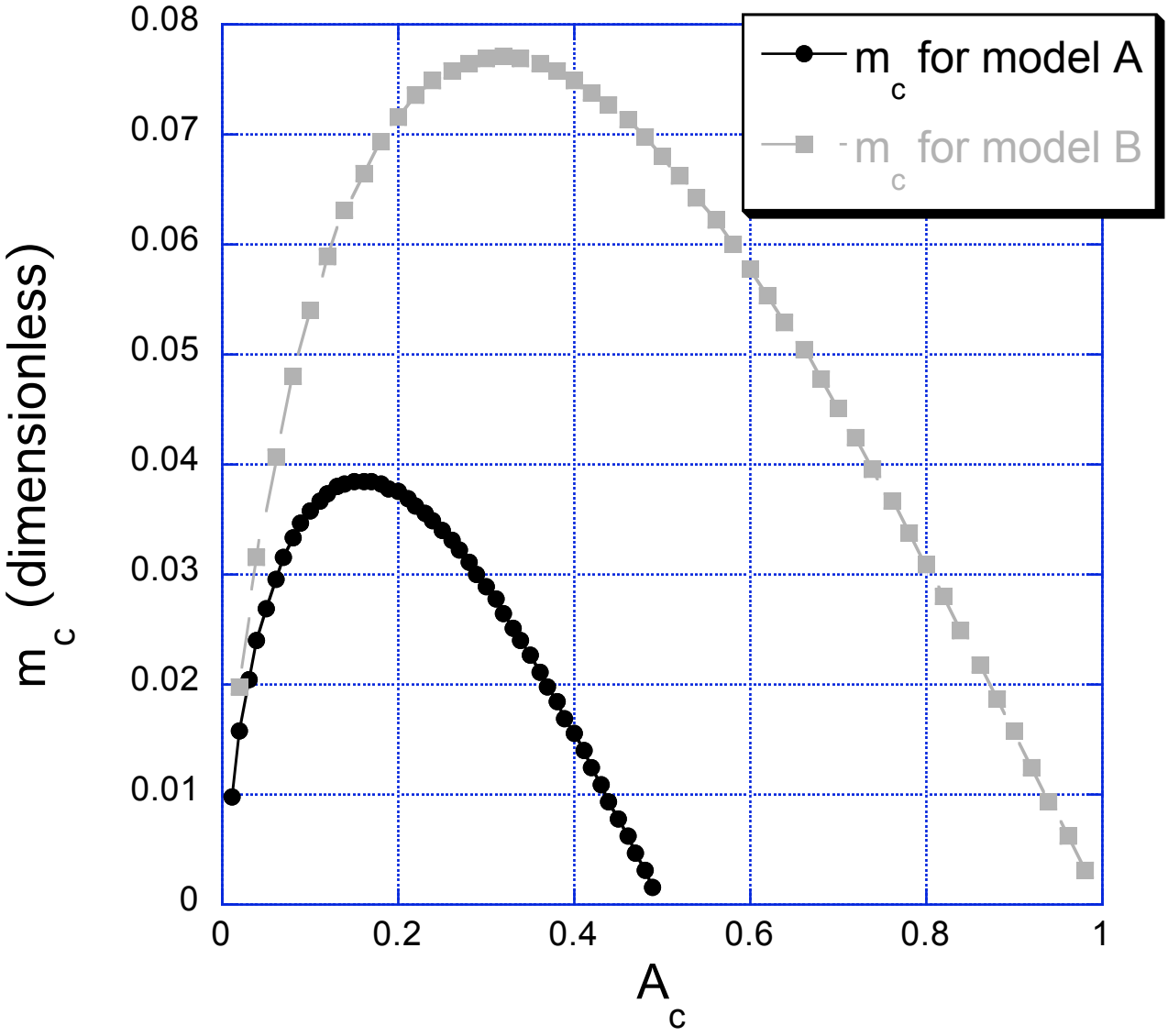

Figure 2. Number of clouds per unit area, m_c (k=1), as a function of cloud fraction A_c for both models A and B.

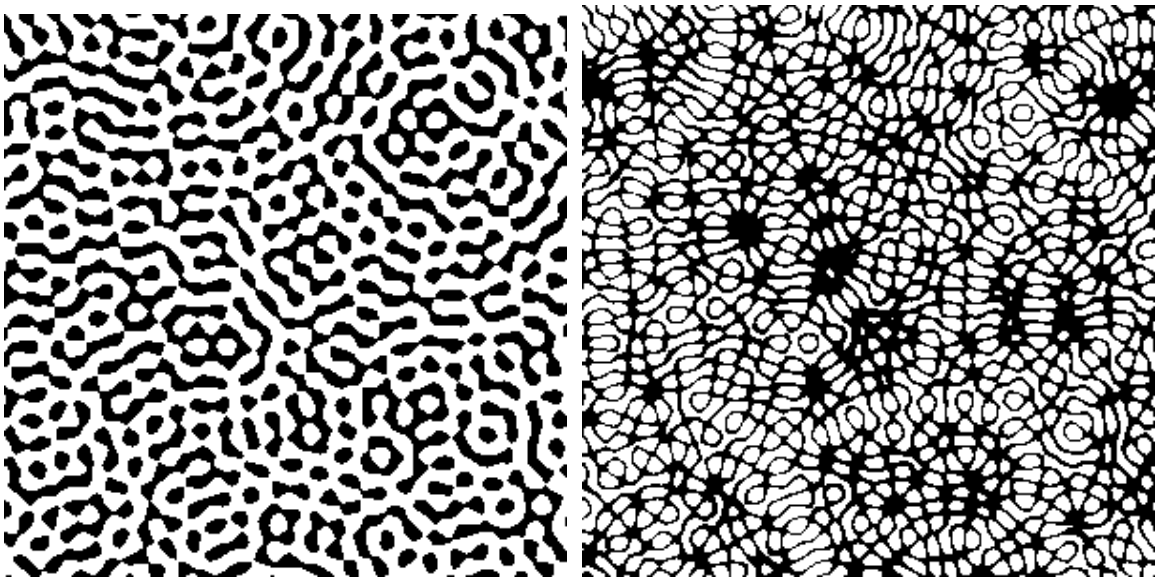

Figure 3. Configuration of cloud fields (300 km by 300 km) for model A (left) and model B (right) on the basis of a Gaussian random field with correlation function J_0 for the same cloud fraction A_c=0.58 (ρ=0.5; d= -0.20 for model A, and d=0.55 for model B). To simulate a Gaussian random field a spectral model from Prigarin, 2001 (Section 1.1.4) was used (see also Appendix B).

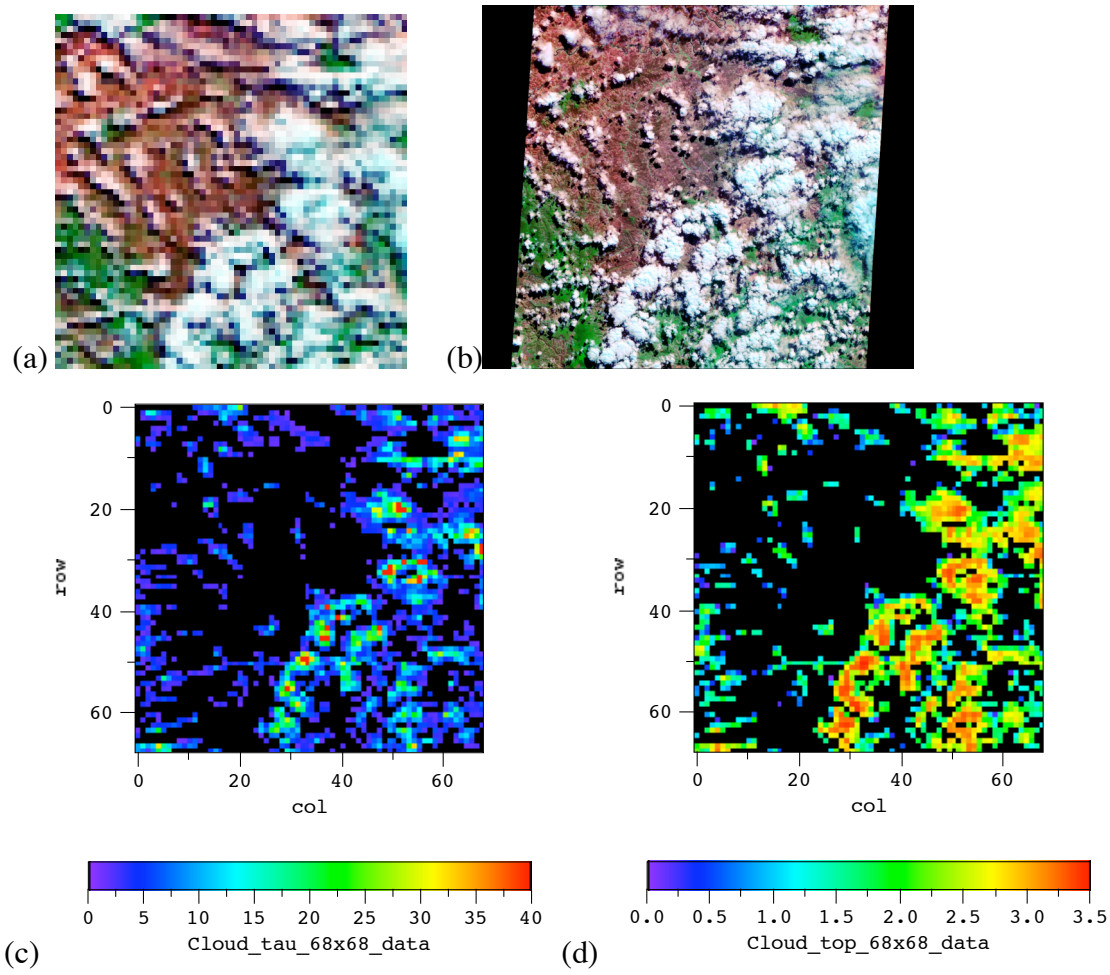

Figure 4. A 68 km by 68 km region in Brazil centered at 17° S and 42° W collected on August 9, 2001 at 1015 local time. The solar zenith angle $\theta_0=41^0$; the solar azimuth angle $\varphi_0=23^o$ (from the top). **(a)** MODIS true color RGB 1 km resolution; **(b)** ASTER RGB 15 m resolution; **(c)** retrieved cloud optical thickness; **(d)** retrieved cloud top height (in km).

Figure 5. Indicator functions $I(x,y)$ of a cloud field: white is cloud (I=1) while black is a cloud-free area (I=0). Cloud fraction A_c=0.4. (**Left**) 68 km by 68 km MODIS image centered at (17.1° S,42.16°W) acquired on August 9, 2001. (**Right**) a realization of a simulated field.

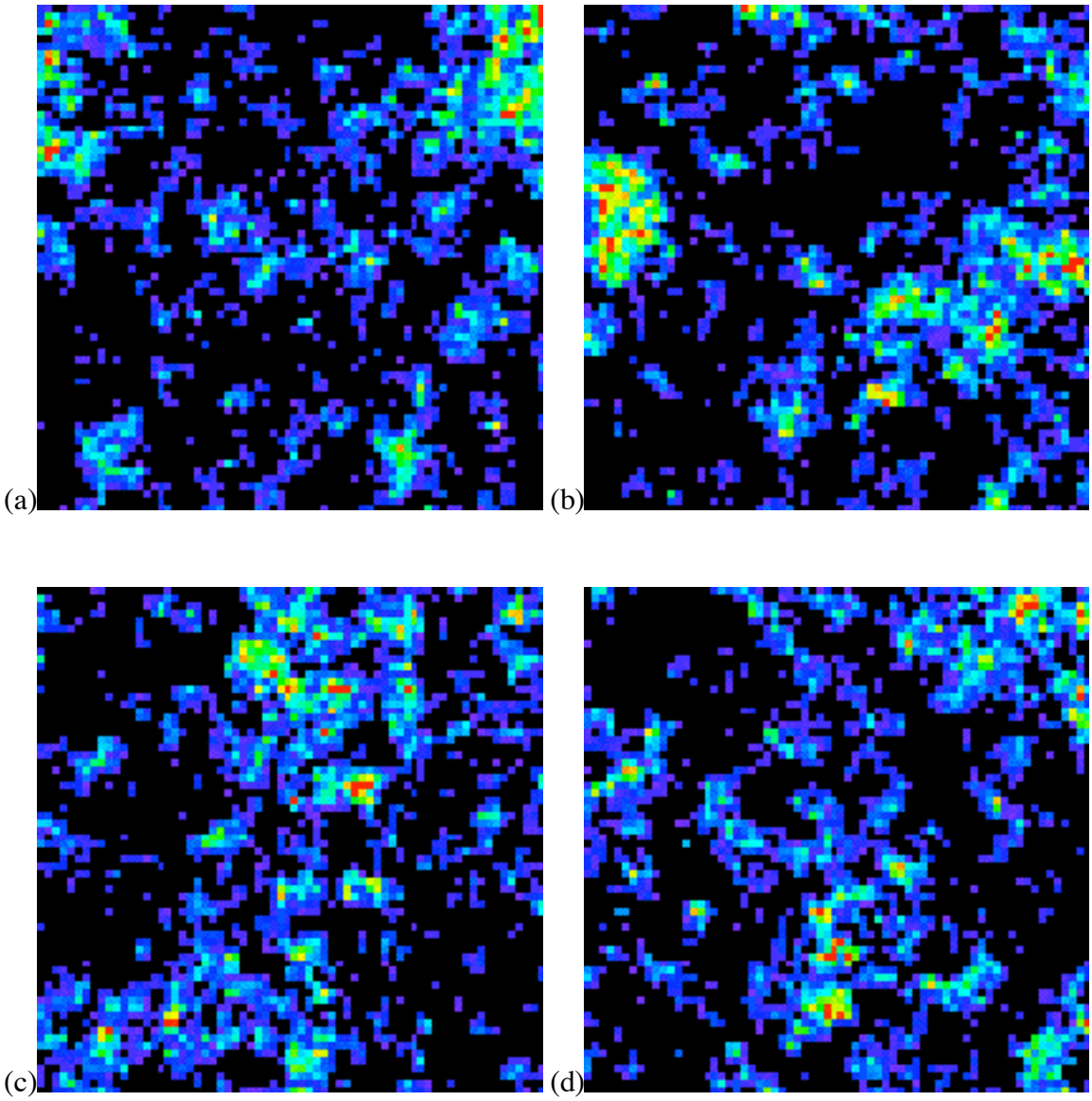

Figure 6. Four realizations of cloud optical depth; all of them have the same covariance function of the cloud mask $K_I(x,y)$ and histogram $g(\tau)$ as the one in Fig. 4c. Color scale is the same as in Fig. 4c. The size of the images is the same as in Fig. 5: 68 km by 68 km.

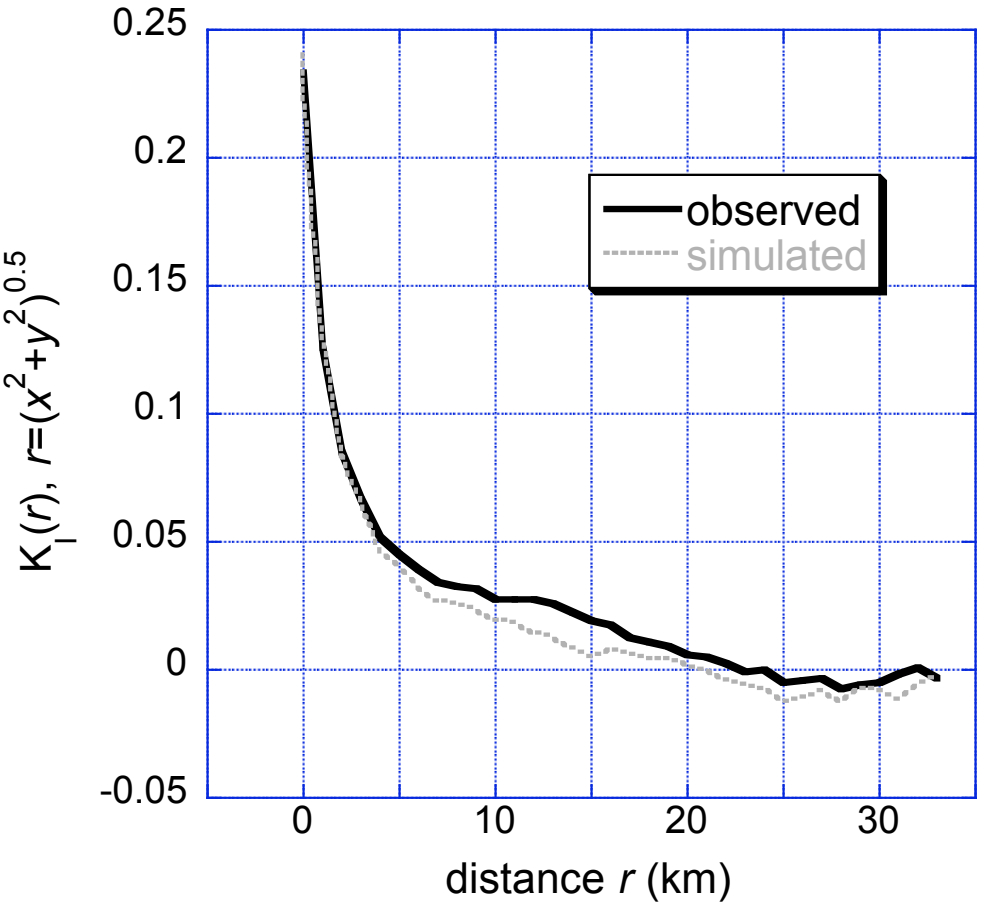

Figure 7. Estimates of covariance function $K_I(x,y)= K_I(r)$ ($r = \sqrt{x^2 + y^2}$) of the indicator function $I(x,y)$ for the observed (solid line) and simulated (dot line) cloud fields from Fig. 5.

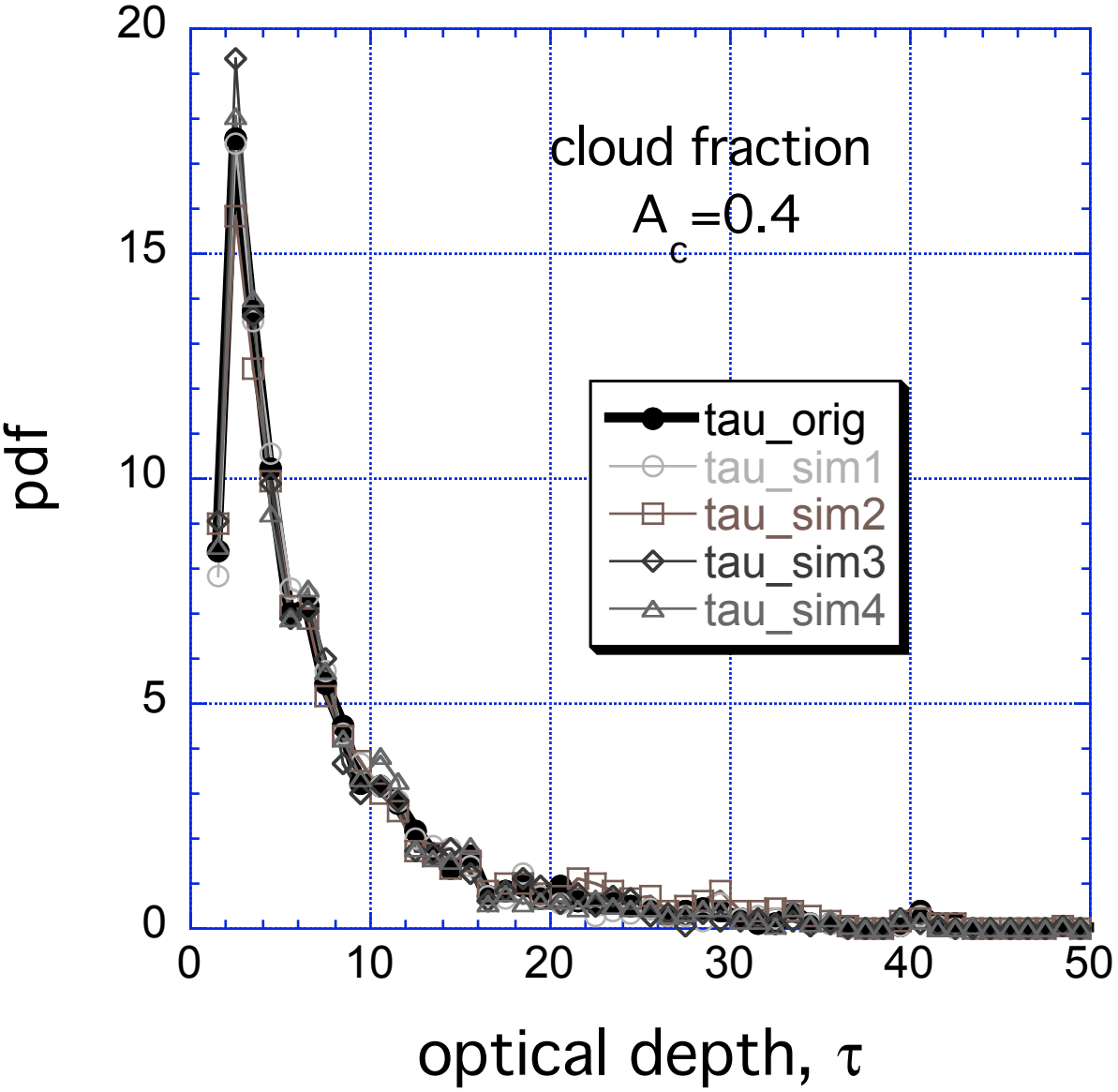

Figure 8. The original histogram g(τ) and four other histograms that correspond to four realizations of cloud optical depth shown in Fig. 6.

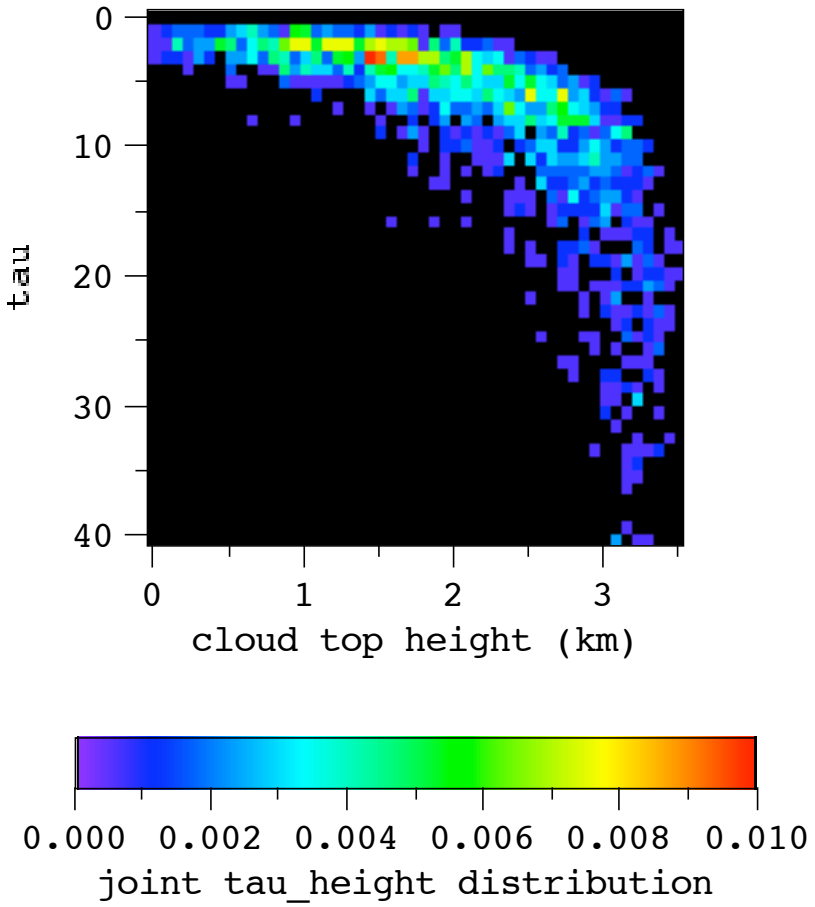

Figure 9. Joint distribution of the given cloud optical depth and cloud top height fields.

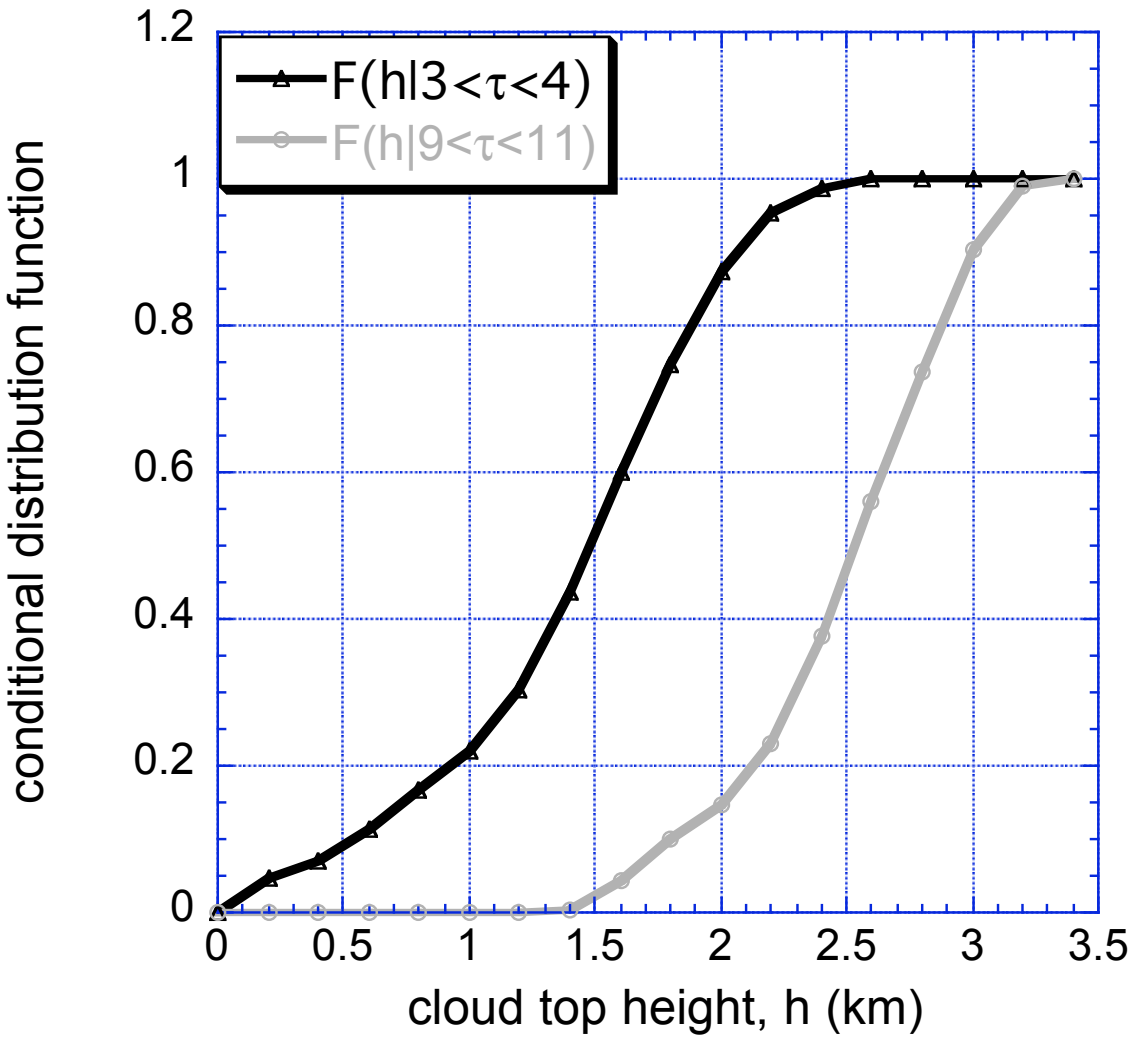

Figure 10. The conditional distribution function $F(h|\tau)$ used to simulate cloud top height h. $F(h|\tau)$ is shown for two values of optical depth τ.

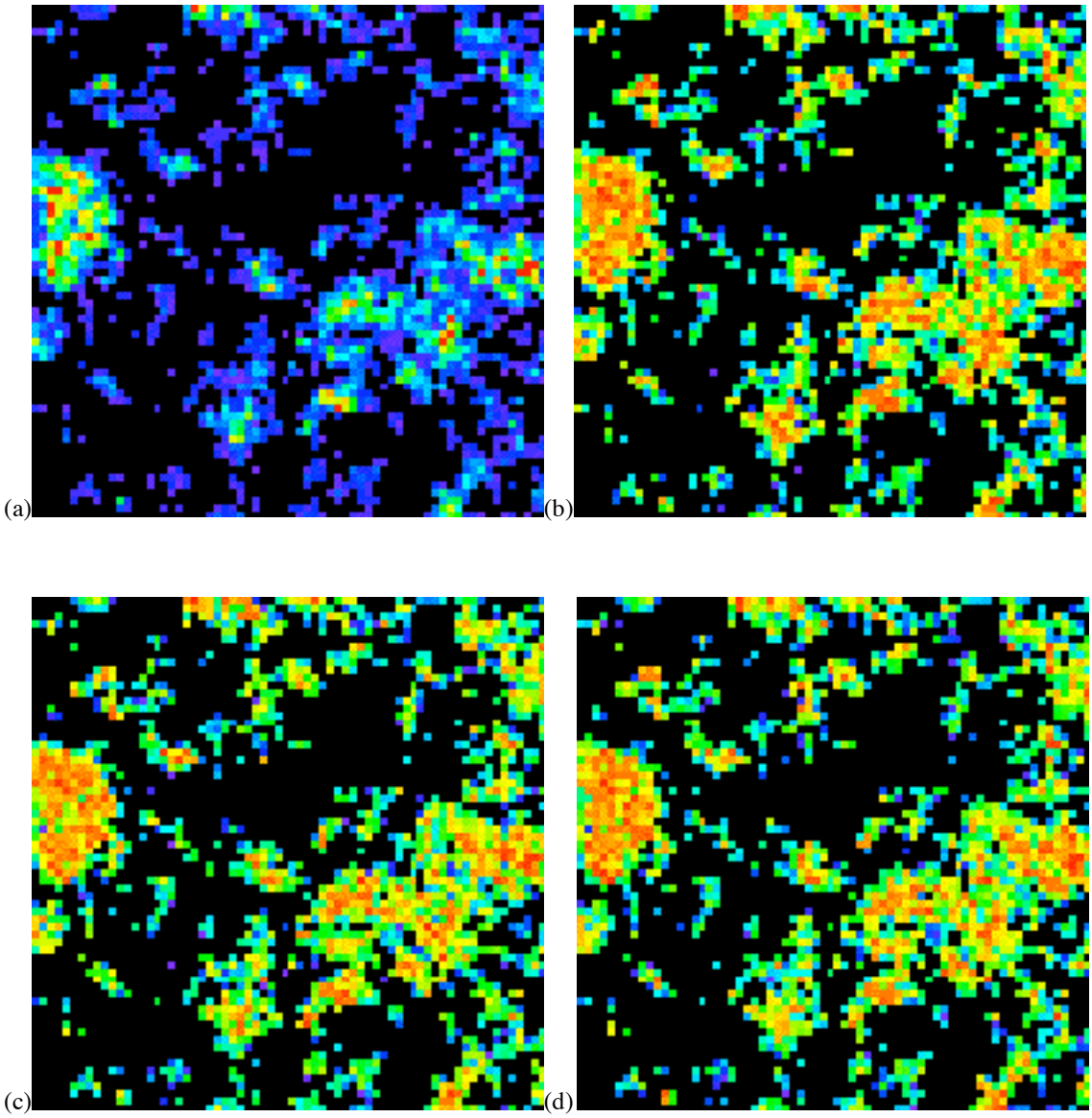

Figure 11. (**a**) One realization of cloud optical depth from Fig. 6b. (**b**)-(**d**) Three realizations of cloud top height distribution; they correspond to the cloud optical depth field shown in panel (a). All realizations have the same conditional distribution $F(h|\tau)$.

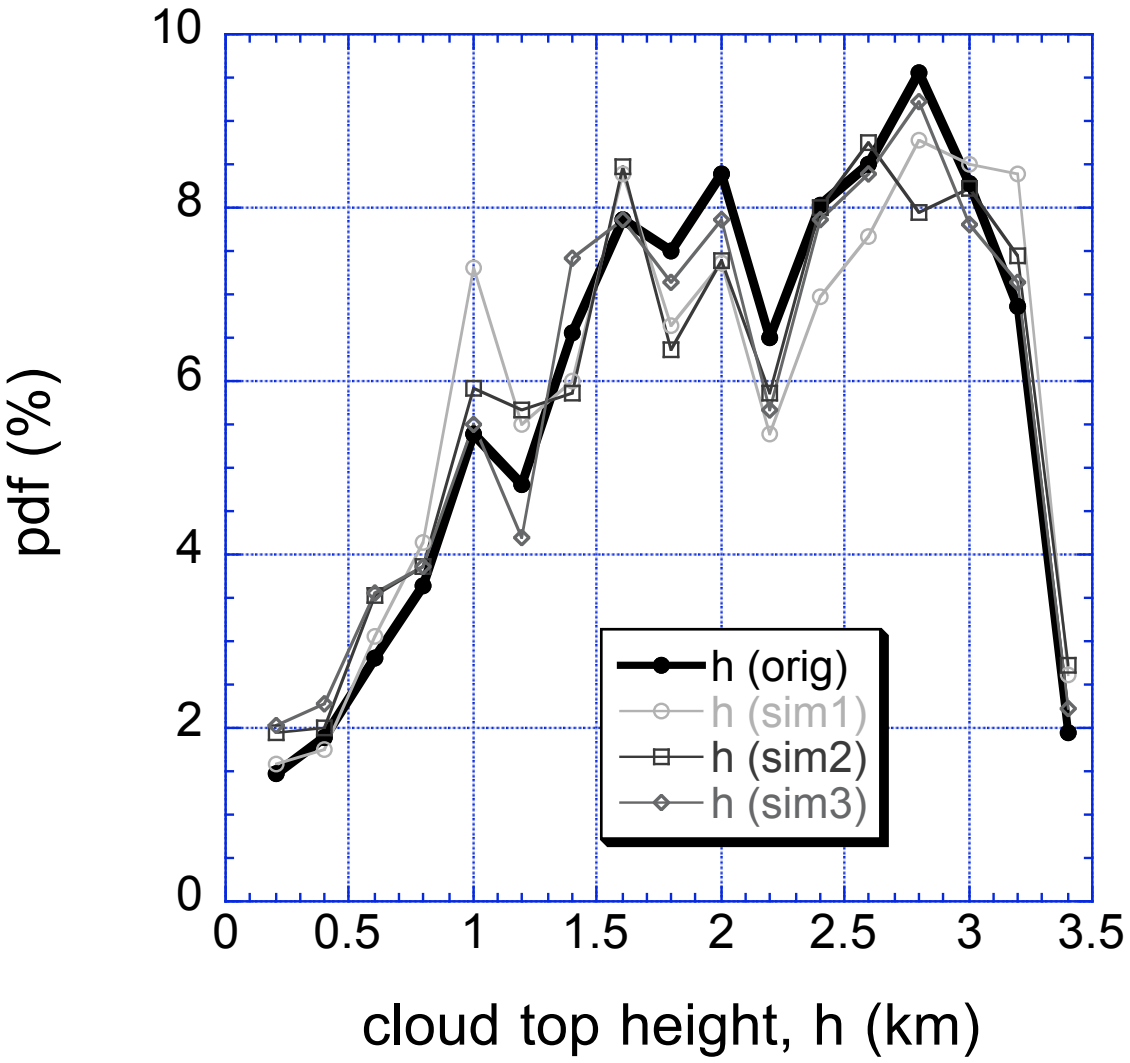

Figure 12. A probability density function (pdf) of three realizations of cloud top height shown in Fig. 11. The original pdf of cloud top height from Fig. 4d is also shown.